J Mater Sci: Mater Electron (2017) 28:11300–11305
DOI 10.1007/s10854-017-6921-7

Optical band gap tuning of Ag doped $Ge_2Sb_2Te_5$ thin films

Palwinder Singh[1,2] · Ramandeep Kaur[1,2] · Pankaj Sharma[3] · Vineet Sharma[3] · Monu Mishra[4] · Govind Gupta[4] · Anup Thakur[2]

Received: 9 March 2017 / Accepted: 7 April 2017 / Published online: 10 April 2017

Abstract Thin films of $(Ge_2Sb_2Te_5)_{100-x}Ag_x$ (x = 0, 1, 3, 5 and 10) were deposited using thermal evaporation technique. X-ray diffraction, scanning electron microscopy and energy dispersive X-ray spectroscopy was used to confirm the amorphous nature, uniformity and chemical compositions of deposited films respectively. Transmission spectra divulged the highly transparent nature of films in near infra red region. The average transmission in near infra red region and optical band gap (estimated by Tauc's plot) was increased with Ag doping upto x = 3 while it decreased for higher values of x. The increase in transmission and optical band gap was attributed to the reduction in density of localized states and vacancies. However, the decrease in the transmission and optical band gap is due to the increase in distortion of the host $Ge_2Sb_2Te_5$ lattice because Ag is doped at the expense of Ge, Sb and Te. The increased optical band gap could be utilized to reduce threshold current which enhances switching speed in phase change materials.

✉ Anup Thakur
dranupthakur@gmail.com; anup_bas@pbi.ac.in

[1] Department of Physics, Punjabi University, Patiala, Punjab 147002, India

[2] Advanced Materials Research Lab, Department of Basic and Applied Sciences, Punjabi University, Patiala, Punjab 147002, India

[3] Department of Physics and Materials Science, Jaypee University of Information Technology, Waknaghat, Solan 173234, India

[4] CSIR-National Physical Laboratory, Advanced Materials and Devices Division, New Delhi 110012, India

1 Introduction

Chalcogenide glasses are the potential candidate for various technological applications due to their unique properties [1–5]. In the last few years, GeTe-based alloys are well studied as phase change materials [3–5] for optical data storage and phase change random access memory (PCRAM) applications. Phase change optical memory devices are based on the reversible phase transformation of the materials between amorphous (low reflectivity) and crystalline (high reflectivity) states. In optical memory devices like CDs, DVDs, Blu-ray etc., data recording is achieved by writing an amorphous state on a crystalline film by local melting with a short pulse of focused and high-intensity laser beam. Rapid cooling of the melt, at rates higher than 10^9 Ks^{-1}, results in amorphous solidification of the state. As an amorphous state has lower reflectivity than the crystalline background therefore detecting (reading) amorphous state is straight forward with a low intensity laser beam. On the other hand, erasing of the state is achieved by heating the amorphous state to temperature above glass transition temperature and allowing the amorphous state to crystallize [6].

On the other hand, PCRAM devices are based on change in resistance upon phase transition of phase change materials. There is a three order of magnitude difference in resistance of amorphous (high resistance, OFF state, RESET) and crystalline (low resistance, ON state, SET) state [7]. In PCRAM, phase transition is retrieved by applying voltage pulse which heats the local state according to Joule's heating. This is non-volatile memory device, in which data recording is done in terms of local structure rather than charge [8]. As the amorphous state has higher resistance so it is considered as RESET operation and crystalline state has lower resistance it is considered as SET operation.

In Ge–Sb–Te ternary diagram, along GeTe–Sb_2Te_3 pseudo binary tie-line, thermal stability increases but crystalline speed decreases [9]. As GeTe is at the end so it has high thermal stability but low crystalline speed, on the other extreme Sb_2Te_3 has low thermal stability but high crystalline speed. $Ge_2Sb_2Te_5$ (GST) is the intermediate candidate on GeTe–Sb_2Te_3 pseudo binary tie-line, so it has good thermal stability and good crystalline speed [9]. Due to better thermal stability, fast crystalline speed, good endurance, scalability and reliability, GST is one of the best phase change material among others. Furthermore, to improve up on these properties of GST, researchers have used different doping materials such as Mg [10], Cr [11], Ni [12], Se [13], Ag [14–16], W [17] etc. Song et al. [14] reported that with Ag doping in GST, the crystalline speed increases from 67 to 30 ns and the sheet resistance increases 10 times in amorphous phase. Phase change materials have a number of properties which are critical for number of applications, including the resistance contrast, transport speed between amorphous and crystalline state and material dependence of the switching characteristics. These are ultimately related to electronic states of the materials [18] which further depend upon their optical band gap.

In the present work, the effect of Ag doping on the optical band gap of amorphous $Ge_2Sb_2Te_5$ thin films has been investigated. As material optical property is strongly dependent on its electronic structure, it is intriguing to tune the optical properties by tuning the optical band gap.

2 Experimental procedure

$(Ge_2Sb_2Te_5)_{100-x}Ag_x$ (x = 0, 1, 3, 5 and 10) bulk alloys have been prepared by melt quenching technique [16, 19]. Thin films of the samples were deposited on glass substrates by thermal evaporation technique using Hind HIVAC system (Model: BC-300) at a deposition rate 10 Å/s under the base pressure of 2.4×10^{-6} mbar. The thickness of thin films was measured by using digital thickness monitor (HHV DTM-101). The detailed procedure of sample preparation was discussed in elsewhere [16]. The amorphous nature of prepared samples was confirmed by X-ray diffraction technique (XRD) using X-ray diffractometer (X'Pert PRO PANalytical) with radiation of Cu $K_{\alpha1}$ ($\lambda = 1.54060$ Å) in the 2θ range 20°–80°. The surface morphology was studied using a JEOL JSM-6510 LV scanning electron microscope (SEM), while the elemental composition was analyzed using INCAx-act, Oxford EDS. Elemental composition of thin film was also verified by X-ray photoelectron (XPS) survey spectra using Omicron Multiprobe Surface Analysis (Scienta Omicron, Germany). MgK_α radiation source (1253.6 eV) along with seven channel detector was employed for XPS data acquisition. The surface contaminants were removed by means of mild sputtering method using 500 eV Ar^+ ions for 10 min. Transmission spectrum of thin films has been taken using UV–Vis-NIR spectrophotometer (Perkin Elmer Lambda 750) in range of 500–3300 nm at room temperature (RT).

3 Results and discussion

Figure 1 shows the XRD patterns for the $(Ge_2Sb_2Te_5)_{100-x}Ag_x$ (x = 0 and 5) films deposited at RT. The patterns do not show any characteristic peaks of Ge–Te, Sb–Te, Ag–Te or $Ge_2Sb_2Te_5$, confirming that films are amorphous in nature. Other films have similar XRD patterns [16]. Figure 2a, b shows the scanning electron microscopic (SEM) images of $(Ge_2Sb_2Te_5)_{100-x}Ag_x$ (x = 0 and 5) thin films which are smooth and uniform. Other films have similar SEM images (results not shown here), especially the surface morphology of the thin films. Furthermore, it is observed that the morphology of the thin films is not much affected with the Ag doping in GST. Figure 2c, d show the local chemical compositions of the $(Ge_2Sb_2Te_5)_{100-x}Ag_x$ (x = 0 and 5) thin film which is characterized by energy dispersive X-ray spectroscopy (EDS). It shows the existence of Ge, Sb, Te and Ag, and the atomic percentages of these elements are very near to the starting elements atomic percentages. EDS has been performed at different locations in the same sample, resulting in the identification of similar chemical composition, which confirms a fairly uniform composition of sample. Other samples have almost-similar composition as that of starting material (results not shown here). The XPS survey scan of the sputter-cleaned $(Ge_2Sb_2Te_5)_{97}Ag_3$ film is shown in Fig. 3 which confirmed the presence of Ge, Sb, Te, and Ag [20], and ruled out the

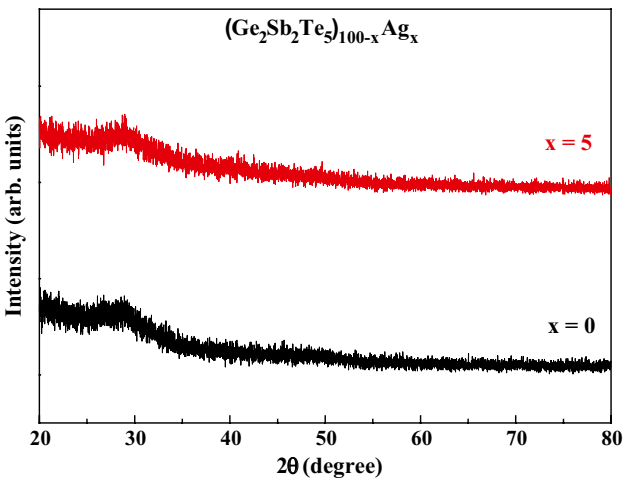

Fig. 1 X-ray diffraction (XRD) patterns of $(Ge_2Sb_2Te_5)_{100-x}Ag_x$ (x = 0 and 5) thin films

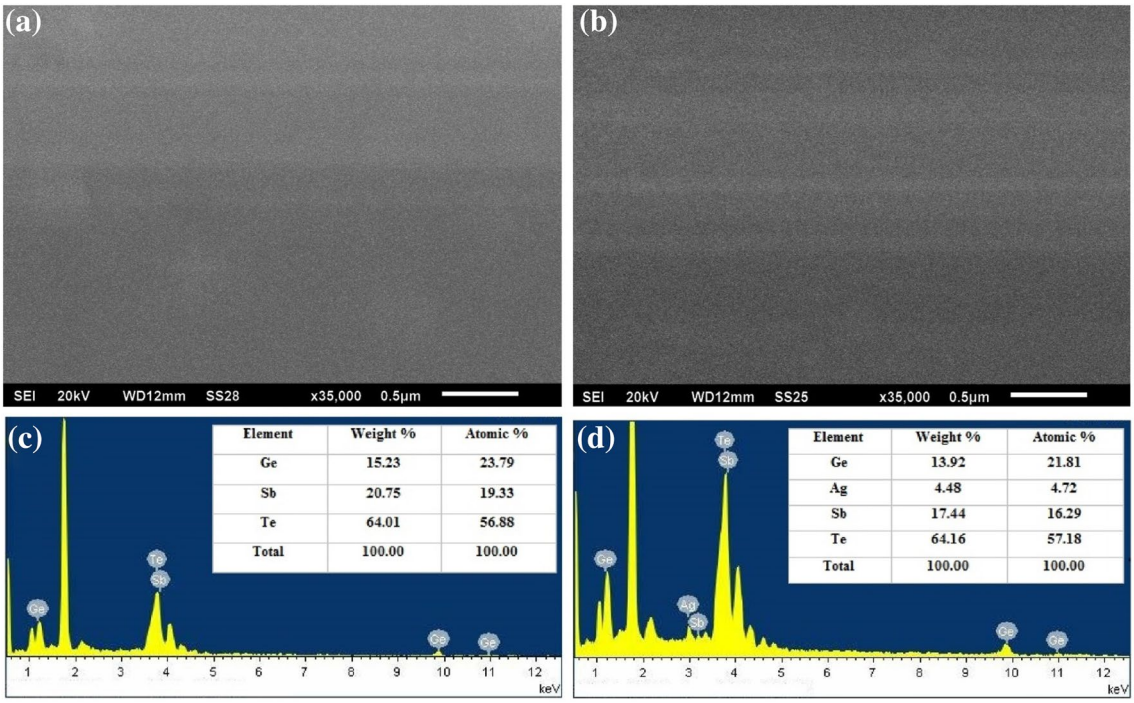

Fig. 2 **a, b** show the scanning electron microscopic images and **c, d** show the energy dispersive X-ray spectra with atomic and weight percentage of constituent elements of $(Ge_2Sb_2Te_5)_{100-x}Ag_x$ (x = 0 and 5) thin films respectively

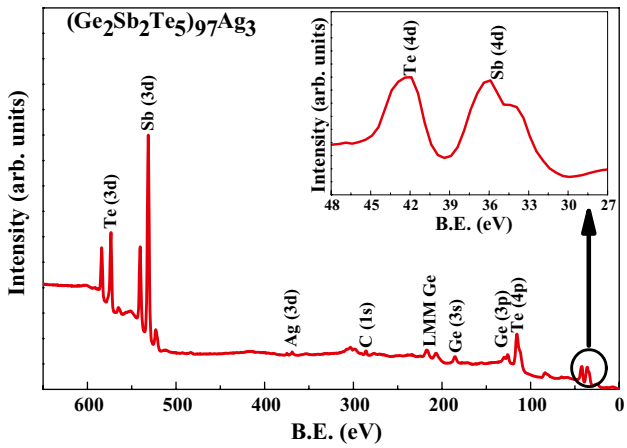

Fig. 3 X-ray photoelectron (XPS) survey spectra of $(Ge_2Sb_2Te_5)_{97}Ag_3$ thin film

incorporation of any other impurity during synthesis. However, some carbon content is detected in the as-deposited thin film (result not shown here), which becomes negligible after sputter cleaning.

The normal-incidence transmission spectra of $(Ge_2Sb_2Te_5)_{100-x}Ag_x$ (x = 0, 1, 3, 5 and 10) thin films are measured by UV–Vis-NIR spectrophotometer in the wavelength range of 500–3300 nm. Inset of Fig. 4 shows the normal incidence set up for transmission measurements. All optical transmission data are normalized to the transmission of bare glass substrate. Figure 4 shows the optical transmission with wavelength for $(Ge_2Sb_2Te_5)_{100-x}Ag_x$ (x = 0, 1, 3, 5 and 10) thin films. The figure shows distinct interference fringes indicating that the films are smooth and uniform [21]. The analysis shows that 3% Ag doped GST film has maximum average transmission in the NIR range confirming minimum density of defect states. The transmission of the films show a relatively sharp absorption edge in near infrared region. A strong absorption normally would occur due to the electronic band transitions of carriers. Figure 4 shows that the absorption edge is shifted towards a lower wavelength till 3% Ag doping and then shifted towards longer wavelength at higher percentages of Ag doping.

Optical absorption coefficient (α) is calculated using the relation $\alpha = [\ln(1/T)]/d$, where T is the transmittance and d is the thickness of thin film. The thickness of deposited thin films is ~700 nm. In high absorption region (where $\alpha \geq 10^4$ cm^{-1}), optical band gap is calculated by Tauc's relation [22]:

$$\alpha h\upsilon = B(h\nu - E_g^{opt})^m \quad (1)$$

where $h\nu$, E_g^{opt} and B denotes the photon energy, optical band gap and band tailing parameter respectively. The value of m depends upon the nature of transition;

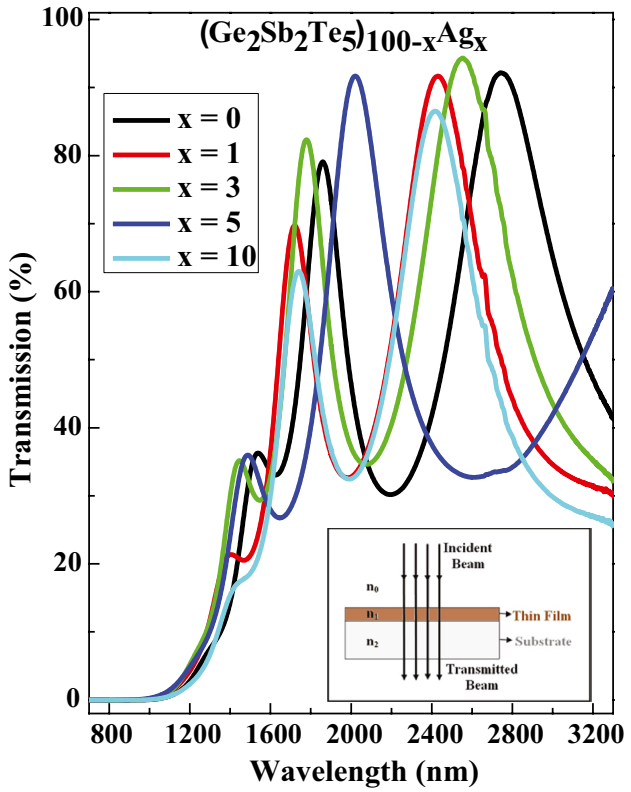

Fig. 4 Transmission spectrum of $(Ge_2Sb_2Te_5)_{100-x}Ag_x$ (x = 0, 1, 3, 5 and 10) thin films and *inset* shows the normal incidence transmission measurement mode where n_o, n_1 and n_2 are the refractive indices of air, thin film and substrate respectively

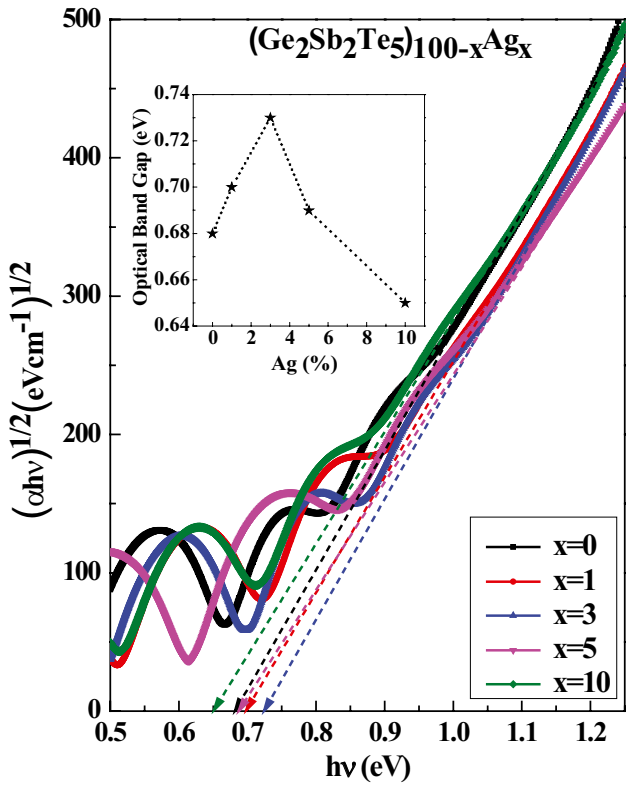

Fig. 5 Variation of $(\alpha h\nu)^{1/2}$ with $h\nu$ for $(Ge_2Sb_2Te_5)_{100-x}Ag_x$ (x = 0, 1, 3, 5 and 10) thin films and *inset* shows the variation of optical band gap with Ag content

for direct allowed transition m is 1/2 for indirect allowed transition m is 2, for direct forbidden transition m is 3/2 and for indirect forbidden transition m is 3. From literature $m = 2$ is acceptable for chalcogenide glasses like GeTe and GeSbTe [23, 24]. The optical bandgap (E_g^{opt}) can be obtained by extrapolating the straight-line portion of $(\alpha h\nu)^{1/2}$ versus $h\nu$ plots to the energy axis. The relationship between $(\alpha h\nu)^{1/2}$ and $h\nu$ for GST films with different Ag doping is shown in Fig. 5, the inset of which illustrates that the optical band gap increases with Ag doping upto 3% and then it starts decreasing. Urbach energy (E_U) is a very important parameter to understand the width of band tail in the forbidden energy gap. The relation between the absorption coefficient, incident photon energy ($h\nu$) and Urbach energy is known as Urbach empirical rule [25] and it is given as:

$$\alpha = \alpha_0 \exp\left[\frac{h\nu}{E_U}\right] \tag{2}$$

here α_0 is constant. Variation of $\ln(\alpha)$ with incident photon energy is given in Fig. 6. Reciprocal of the slope of this straight line gives the value of Urbach energy. Inset of Fig. 6 shows the variation of Urbach energy with Ag content. With Ag doping upto 3% E_U decreases and then increases for higher Ag content.

Generally, materials show a blue or a red shift on doping due to decrease or increase in gap states in chalcogenide glasses, respectively. The increase in optical band gap with Ag doping upto 3% can be understood from the decrease of density of localized states in the band gap. These localized states are responsible for number of effects in amorphous materials like structural, magnetic, optical etc. The presence of these localized states in gap has been discussed in various models [26–31]. According to these models, there are donor (D^-) as well as acceptor (D^+) defect states present near the Fermi level (represented by E_x and E_y in Fig. 7). These defect states are also known as wrong bonds or dangling bonds. The density of these states is very large ~10^{18} cm^{-3} [27]. The width of band tail near mobility edge depends upon the density of defect states in the amorphous materials [32]. Chaudhuri et al. [33] reported that when Ag is doped in chalcogenide glasses, it is weakly bonded and neutral but in trapping centre it is Ag^+ state. So doping of Ag in chalcogenide glasses convert charged defect states into neutral states in trapping centres as follow [32].

$$D^+ + e^- \rightarrow D^0 \tag{3}$$

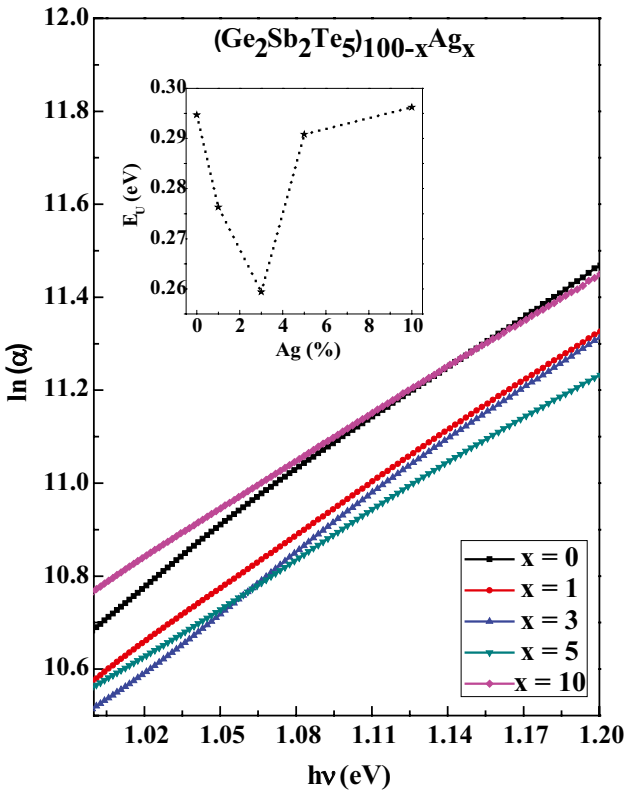

Fig. 6 Variation of ln(α) with $h\nu$ for $(Ge_2Sb_2Te_5)_{100-x}Ag_x$ (x = 0, 1, 3, 5 and 10) thin films and *inset* shows the variation of Urbach energy (E_U) with Ag content

$$D^- + Ag^+ \rightarrow [D^- Ag^+]^0 \quad (4)$$

In this way, Ag doping reduces the density of charged defect states in GST. Due to this, disorder in the material decreases which causes decrease in the width of band tailing near mobility edge as shown in Fig. 7. Urbach energy results also show the decrease in the width of band tailing near mobility edge (E_V to E_B and E_C to E_A in Fig. 7). Increase in transmission with Ag doping also confirm the decrease in width of band tailing near mobility edge. Hence the optical band gap increases with Ag doping upto 3% and decreases for higher Ag doping. This decrease in the optical band gap is due to the increase in distortion of the host GST lattice because Ag is doped at the expense of Ge, Sb and Te. Singh et al. [16] reported the distortion in GST host matrix with Ag doping at higher content in their recently published work. It is verified by Raman spectroscopy that Raman band at ~124 cm^{-1} and ~152 cm^{-1} are present in host and Ag doped GST up to 3% content which are assigned to $GeTe_{4-n}Ge_n$ (n = 1,2) corner sharing tetrahedral and Sb-Te vibrations in $SbTe_3$ unit or from defective octahedral coordination of Sb atoms respectively. Structural distortion at higher Ag content is confirmed from the decrease in intensity of these bands.

Increase in optical band gap is very important in order to reduce threshold current which enhances switching speed and gives better thermal stability in phase change materials [34]. Enlarged band gap also increases signal to noise ratio, which gives large resistance contrast and due to this the data readability gets improved in PCRAM devices [14].

4 Conclusions

$(Ge_2Sb_2Te_5)_{100-x}Ag_x$ (x = 0, 1, 3, 5 and 10) bulk alloys have been prepared by melt quenching technique. Thin films of these samples were deposited on glass substrate using thermal evaporation technique. From transmission spectrum of deposited thin films, optical band gap was calculated using Tauc's plot. The increase in optical band gap upto 3% Ag doping was due to reduction in density of defect states and

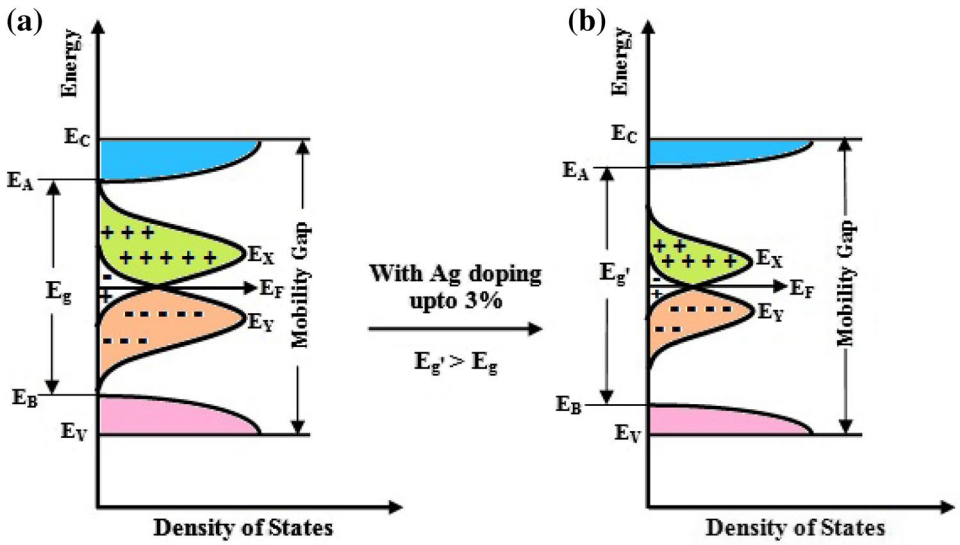

Fig. 7 Schematic illustration of change in the optical band gap with Ag doping in $Ge_2Sb_2Te_5$ using density of localized states in the band gap

decrease in depth of band tails. At higher percentage of Ag doping the band gap decreases due to distortion in the host GST lattice. Increase in optical band gap could be important factor to reduce threshold current which enhances switching speed in phase change materials. In this way, we can tune the transmission band over a wide range of frequencies.

Acknowledgements This work is financially supported by Department of Science and Technology, New Delhi under Research Project (Sanction No. SB/FTP/PS-075/2013 dated 29/05/2014). PS is thankful to Department of Science and Technology, New Delhi for providing financial support as SRF under above mentioned Research Project.

References

1. R.P. Tripathi, M.S. Akhtar, M.A. Alvi, S.A. Khan, J. Mater. Sci. **27**, 8227–8233 (2016)
2. B. Zheng, Y. Sun, J. Wu, L. Yuan, X. Wu, K. Huang, S. Feng, J. Nanopart. Res. **19**, 50 (2017)
3. S. Raoux, W. Welnic, D. Ielmini D, Chem. Rev. **110**, 240–267 (2010)
4. H.C. Lee, J.H. Jeong, D. Choi, Semicond. Sci. Technol. **31**, 095006 (2016)
5. J.E. Boschker, M. Boniardi, A. Redaelli, H. Riechert, R. Calarco, Appl. Phys. Lett. **106**, 023117 (2015)
6. M. Wuttig, N. Yamada, Nat. Mater. **6**, 824–832 (2007)
7. I. Friedrich, V. Weidenhof, W. Njoroge, P. Franz, M. Wuttig, J. Appl. Phys. **87**, 4130 (2000)
8. R. Bez, A. Pirovano, Mat. Sci. Semicon. Proc. **7**, 349–355 (2004)
9. E.M. Vinod, K. Ramesh, K.S. Sangunni, Sci. Rep. **5**, 8050 (2015)
10. J. Fu, X. Shen, Q. Nie, G. Wang, L. Wu, S. Dai, T. Xu, R.P. Wang, Appl. Surf. Sci. **264**, 269–272 (2013)
11. Q. Wang, B. Liu, Y. Xia, Y. Zheng, R. Huo, Q. Zhang, S. Song, Y. Cheng, Z. Song, S. Feng, Appl. Phys. Lett. **107**, 222101 (2015)
12. Y. Zhu, Z. Zhang, S. Song, H. Xie, Z. Song, X. Li, L. Shen, L. Li, L. Wu, B. Liu, Mater. Res. Bull **64**, 333–336 (2015)
13. E.M. Vinod, K. Ramesh, R. Ganesan, K.S. Sangunni, Appl. Phys. Lett. **104**, 063505 (2014)
14. K.H. Song, S.W. Kim, J.H. Seo, H.Y. Lee, J. Appl. Phys. **104**, 103516 (2008)
15. B. Prasai, G. Chen, D.A. Drabold, Appl. Phys. Lett. **102**, 041907 (2013)
16. P. Singh, P. Sharma, V. Sharma, A. Thakur, Semicond. Sci. Technol. **32**, 045015 (2017)
17. S. Guo, X.J. Ding, J.Z. Zhang, Z.G. Hu, X.L. Ji, L.C. Wu, Z.T. Song, J.H. Chu, Appl. Phys. Lett. **106**, 052105 (2015)
18. D. Ielmini, Y.G. Zhang, J. Appl. Phys. **102**, 054517 (2007)
19. A. Thakur, V. Sharma, P.S. Chandel, N. Goyal, G.S.S. Saini, J. Mater. Sci. **41**, 2327–2332 (2006)
20. J.F. Moulder, W.F. Stickle, P.E. Sobol, K.D. Bombea, *Handbook of X-ray Photoelectron Spectroscopy*, ed. by J. Chastain, (Perkin-Elmer Corporation, USA, 1992)
21. A. Thakur, H. Yoo, S.J. Kang, J.Y. Baik, I.J. Lee, H.K. Lee, K. Kim, B. Kim, S. Jung, J. Park, H.J. Shin, ECS J. Solid State Sci. Technol. 1(1), Q11–Q15 (2012).
22. J. Tauc, *The Optical Properties of Solids*. (North-Holland, Amsterdam, 1970)
23. B.S. Lee, J.R. Abelson, S.G. Bishop, D.H. Kang, B.K. Cheong, K.B. Kim, J. Appl. Phys. **97**, 093509 (2005)
24. H.Y. Lee, J.W. Kim, H.B. Chung, J. Non-Cryst. Solids **315**, 288–296 (2003)
25. F. Urbach, Phys. Rev. **92**, 1324 (1953)
26. M.H. Cohen, H. Fritzsche, S.R. Ovshinsky, Phys. Rev. Lett. **22**, 1065 (1969)
27. N.F. Mott, E.A. Davis, R.A. Street, Philos. Mag. **32**(5), 961–996 (1975)
28. E.A. Davis, N.F. Mott, Philos. Mag. **22**, 903–922 (1970)
29. N.F. Mott, Philos. Mag. **24**, 935–958 (1971)
30. D. Krebs, T. Bachmann, P. Jonnalagadda, L. Dellmann, S. Raoux, New J. Phys. **16**, 043015 (2014)
31. R. Kaur, P. Singh, K. Singh, A. Kumar, A. Thakur, Superlattices Microstruct. **98**, 187–193 (2016)
32. S. Kumar, D. Singh, R. Thangraj, Thin Solid Films **540**, 271–276 (2013)
33. I. Chaudhuri, F. Inam, D.A. Drabold, Phys. Rev. B **79**, 100201(R) (2009)
34. W. Welnic, A. Pamungkas, R. Detemple, C. Steimer, S. Blugel, M. Wuttig, Nat. Mater. **5**, 56–62 (2006)